RESEARCH ARTICLE

NANO · MICRO small
www.small-journal.com

Nickel Oxide/Cobalt Phthalocyanine as a Hole Transport Bilayer for Efficient and Stable Inverted Perovskite Solar Cells

*Meiirkhan Beisembekov, Aitbek Aimukhanov, Serzhan Tazhibayev, Dosmukhammed Abeuov, and Assylbek Zeinidenov**

This study demonstrates that the use of bilayer films based on nickel oxide (NiO_x;) and cobalt phthalocyanine (CoPc) represents a promising hole transport layer (HTLs) for inverted perovskite solar cells (PSCs). NiO_x; films are fabricated using the spin-coating method from a sol–gel solution. Films ($CoPc_{evap}$) and nanowires ($CoPc_{nws}$) on the NiO_x; surface are produced by thermal sputtering and physical gradient-temperature vapor deposition. It is demonstrated that PSCs with a NiO_x; layer exhibit a power conversion efficiency (PCE) of only 18,1%. The incorporation of a $CoPc_{evap}$ intermediate layer between NiO_x; and the perovskite increases the PCE to 19.1%. The highest PCE, reaching 20.7%, is achieved with a bilayer HTLs based on NiO_x;/$CoPc_{nws}$. Analysis of the PSC impedance spectra shows that the $CoPc_{nws}$ intermediate layer reduces the HTLs resistance and increases the recombination resistance at the perovskite/HTLs interface, which extends the effective lifetime of charge carriers. The stability of NiO_x;-based PSCs is 48%, while PSCs with bilayer HTLs based on NiO_x;/$CoPc_{nws}$ and NiO_x;/$CoPc_{evap}$ exhibits higher stability of 71% and 90% over 600 hours. The results demonstrated that solar cells based on NiO_x;/CoPc inhibit the perovskite degradation process and reduce charge recombination, thereby improving the performance and stability of the inverted PSCs.

1. Introduction

NiOx is one of the most promising hole transport materials for inverted PSCs. The PCE of NiO_x;-based inverted PSCs has exceeded 20%. These results were achieved due to the simplicity of synthesis, a wide bandgap (>3.5 eV), a favorable valence band maximum (VBM ≈5,4 eV), and superior chemical stability compared to other inorganic materials.[1,2,3] Although NiO_x; thin films serve as a promising HTLs in PSCs, the efficiency of NiO_x;-based PSCs remains slightly lower than that of PSCs using Spiro-OMeTAD and crystalline silicon solar cells. The limited hole transport capability of NiO_x; leads to inefficient charge carrier separation and transport at the NiO_x;/perovskite heterojunction, making NiO_x;-based inverted PSCs less competitive compared to other solar cells.[4,5]

To enhance the efficiency and stability of inverted PSCs, research is being conducted to develop new and effective materials for the HTLs. Recent studies have shown that charge transport properties at the perovskite/HTLs interface are the key factor limiting the efficiency and stability of PSCs.[6,7] For instance, in,[8] NiO_x; HTLs films treated with oxygen were fabricated, resulting in PSCs with an efficiency of up to 17%. The authors of[9] reported inverted PSCs with a NiO_x; layer obtained without annealing, achieving a PCE of 20.9%. In,[10] the superior electronic properties of the CBD-NiO_x; HTLs enabled inverted PSCs to reach a PCE of 23.30%. Therefore, the choice of HTLs is crucial not only for charge transport and device efficiency but also for perovskite protection and overall device stability.[11–13]

Recently, efforts have been made to develop bilayer HTLs materials to improve the photovoltaic performance and stability of PSCs.[14,15] For example, Mali et al. reported that NiO_x;/CuSCN double HTLs devices increased the PCE from 14.46% to 19.24%.[16] In,[17] a bilayer NiO_x;/Spiro film was developed. The results showed that PSCs based on the NiO_x;/Spiro HTLs exhibited faster hole extraction and better energy level alignment compared to pure Spiro, thereby improving the PCE from 19.8% to 21.66%.

For efficient hole transport through the HTLs, the material's functional characteristics must be well aligned with the valence band level of the perovskite. This alignment is crucial to minimize the hole transport barrier and prevent recombination. Therefore, selecting materials with an appropriate work function is essential to ensure effective contact with the perovskite active layer.It is well known that 1D nanostructures, such as nanowires, nanorods, or nanotubes, can play a significant role in improving conductivity and hole transport in the HTLs. These structures provide high conductivity and an efficient charge transport pathway. Additionally, they can enhance the mechanical flexibility and durability of the device, which is

M. Beisembekov, A. Aimukhanov, S. Tazhibayev, D. Abeuov, A. Zeinidenov
Scientific Center of nanotechnology and functional nanomaterials
Buketov Karaganda University
University str., 28, Karaganda 100028, Kazakhstan
E-mail: Zeinidenov_Assylbek@buketov.edu.kz

The ORCID identification number(s) for the author(s) of this article can be found under https://doi.org/10.1002/smll.202501794

DOI: 10.1002/smll.202501794

important for the long-term stability of solar cells.Furthermore, the typical porous structure of these nanomaterials is beneficial for effective perovskite infiltration, as well as for improving light harvesting and charge extraction. Extensive research on various 1D nanostructures as electron transport layers in advanced mesoporous p-i-n devices has demonstrated their great potential.[18,19]

One promising class of macrocyclic compounds is metal phthalocyanines (MPc). These compounds are chemically and thermally stable, exhibit significant optical absorption in the visible spectrum, and easily form ordered thin films with high photoconductivity. The physical and chemical properties of MPc are well-regulated by optimizing the central metal ions and their structure (size, shape). It is worth noting that MPc do not interact with strong acids, are virtually unaffected by air up to temperatures of 400–500 °C, and, in a vacuum, most phthalocyanines do not decompose up to 900 °C. Phthalocyanines do not degrade as rapidly under light exposure, which is often accompanied by the release of iodine compounds, in contrast to the degradation observed in perovskite materials.[20]

The effectiveness of using MPc in PSCs with a p-i-n configuration has been confirmed by several research groups. For example, the authors of[21] achieved a PCE of up to 20%. These results were obtained by depositing a CoPc layer on a perovskite film with a specific orientation. Recently, the best efficiency values for PSCs have been achieved using NiPc as a dopant-free material with hole conductivity. The authors achieved a record PCE of 21.23%, and the PSCs also demonstrated good photostability, as well as resistance to moisture and heating.[22] Liao and colleagues were the first to demonstrate the use of CoPc as a HTLs in inverted PSCs. Solar cells with the structure ITO/CoPc/$MAPbI_3$/PCBM/BCP/Ag were fabricated, achieving a solar energy conversion efficiency of 14.5%. Additionally, the devices exhibited good stability in the atmosphere (temperature: 20–25 °C and relative humidity: 40–50%) without encapsulation.[23] In,[24] nickel phthalocyanine (NiPc) was used for the first time as a hole transport material in inverted planar perovskite solar cells. An energy conversion efficiency of 14.3% was achieved. Moreover, the inverted planar PSCs based on NiPc exhibit very weak hysteresis. Zhao and co-authors developed photoconductive HTLs using NiO_x; with phthalocyanine (Pc). It was shown that under illumination, the Pc molecule absorbs light and becomes excited. The photogenerated charges on the Pc molecule then spontaneously transfer to the NiO_x;, increasing the hole density in the NiO_x; film, thereby improving its conductivity. As a result, an increase in conductivity was observed in the NiO_x;- Pc film. PSCs with NiO_x;-Pc demonstrated a high efficiency of 21.68%, significantly higher than the control cells (19.74%).[25]

In this study, we have obtained highly efficient and stable PSCs based on bilayer hole-transport layers of NiO_x; and CoPc. The results of investigation of the influence of CoPc films and nanowires on the efficiency of charge generation and transport in PSCs are presented.

In this work, we have developed highly efficient and stable PSCs based on bilayer HTLs of NiO_x; and CoPc. The results of the study on the influence of CoPc films and nanowires on charge generation and transport efficiency in PSCs are presented.

2. Experimental Section

2.1. Sample Preparation and Deposition Process

2.1.1. Composition of HTLs

NiOx films on the surface of a solid substrate were prepared from solutions of [$Ni(NO_3)_2 \cdot 6H_2O$] (m = 145 mg) in ethylene glycol (V = 1 ml). To the resulting solution, (5 µl) of monoethanolamine was added. The solution was stirred at room temperature for 16 hours, and then left to stand for 24 hours. NiO_x; films were obtained using the sol-gel method with a substrate rotation speed of 1500 rpm on a SPIN150i centrifuge (Semiconductor Production System). The obtained films were pre-annealed at 100 °C for 15 minutes. Afterward, the films were annealed in air at temperatures of 300 °C for 45 minutes.

2.1.2. Preparation of Bilayer HTLs

Cobalt phthalocyanine (Sigma-Aldrich) was used as the HTLs. The CoPc layer on the NiO_x; surface was deposited by thermal evaporation in a vacuum using the CY-1700x-sps-2 system (Zhengzhou CY Scientific Instruments Co., Ltd). The residual pressure in the working chamber during operation did not exceed 10^{-5} Pa. A rotating drive was used to achieve a uniform thickness during evaporation. To enhance the crystallinity of the films, the evaporation rate of the phthalocyanine molecules was kept below 1 nm/s. By lowering the deposition rate, the quality of the films improves since the phthalocyanine molecules have more time to reach thermodynamic equilibrium before being tightly fixed by the subsequent layer of molecules.[26]

The preparation of nanowires on the NiO_x; surface was carried out using the physical gradient-temperature vapor deposition (TG-PVD) method in an argon atmosphere. A small amount of phthalocyanine was placed in a ceramic crucible and positioned inside a quartz tube in the heating zone. The working volume of the tube was then filled with argon (99.999%). For circulation of the inert gas, the working volume of the setup was evacuated using a vacuum pump. The flow rate of argon in the reaction zone was 150 cm^3 min^{-1}. The working zone was then heated to a temperature of 440–470 °C. The temperature of the working zone was monitored using a PID controller with a type K thermocouple. The scheme for preparing bilayer HTLs was shown in **Figure 1**.

2.1.3. Perovskite Materials

The perovskite was prepared using $PbCl_2$ (Sigma-Aldrich) and Methylammonium iodide (MAI). The photoactive layer was obtained by dissolving $PbCl_2$ powder (230 mg) and MAI (394 mg) in 1 ml of N,N-Dimethylformamide (Sigma-Aldrich). The resulting solution was stirred with a magnetic stirrer at 60 °C for 2 hours. After film deposition, the perovskite films were annealed for 2 hours at 90 °C to ensure complete crystallization. The crystallization process was accompanied by a color change of the film from yellow to dark brown.

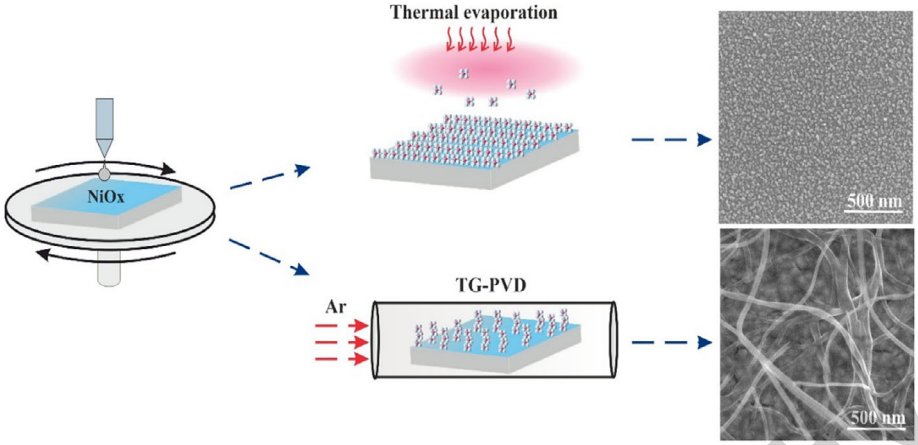

Figure 1. Schematic representation of the preparation of bilayer HTLs.

2.1.4. Fabrication of Solar Cells

Inverted PSCs were fabricated on glass substrates coated with a thin conductive FTO layer (Biotain Hong Kong Co., FTO thickness – 105 nm, R < 15 Ω cm^{-2}, transparency 81–83.5%). A NiO_x; film was applied to the FTO-coated substrate using the sol-gel method from the solution. Then, solid CoPc films and nanowires were sequentially synthesized on the NiO_x; surface. Afterward, the photoactive perovskite layer was applied to the NiO_x;/CoPc bilayer structure. In the next step, an ETL layer of PC61BM:BCP was applied to the perovskite surface using the spin-coating method. Finally, an Ag electrode was sputtered onto the surface of the films under a vacuum of 10^{-3} Pa. To minimize oxidation, all operations were carried out in a sealed glovebox.

2.2. Analysis Methods

The surface topography of the samples was studied using an atomic force microscope JSPM-5400 (AFM, JEOL). Data processing of the images obtained from the AFM was carried out using a specialized modular program for scanning probe microscopy data analysis (WinSPMII Data-Processing Software).

The crystal structure of the samples was investigated using X-ray diffraction (XRD) methods. XRD measurements were performed using the RigakuMiniFlex X-ray diffractometer (Japan).

Raman scattering spectra were measured using the Gurzil Raman Microscope TO-RM-S-532 / TO-RM-S-785 (Thunder Optics, France). A semiconductor laser (Thunder Optics, France) with a wavelength of 785 nm and a line width of 0.03 nm was used to excite the spectra.

Absorption spectra of the samples were recorded using the AvaSpec-ULS2048CL-EVO spectrometer (Avantes). The light source used was a combined deuterium-halogen light source AvaLight-DHc (Avantes), with a working range of 200–2500 nm.

The photoluminescence decay kinetics were measured using a pulsed spectrofluorometer with picosecond resolution and photon-counting mode registration.

The current-voltage (I-V) characteristics of the photovoltaic cells were determined using the Sol3A Class AAA Solar Simulators (Newport) with the PVIV-1A I-V Test Station.

The impedance spectra were measured using the P45X potentiostat-galvanostat in impedance mode, with an additionally installed FRA-24 M frequency analyzer module. The error in determining the parameters of charge carrier transport did not exceed 5%, and was predominantly 1–1.5%. Fitting and analysis of the spectral parameters were carried out using the EIS-analyzer software according to the procedure described in.[27]

3. Results and Discussion

3.1. Surface Morphology

At the first stage of the work, thin NiO_x films were obtained using the spin-coating method. As seen in **Figure 2**a, the surface morphology of the NiO_x film exhibits a uniform granular structure with a surface roughness (Ra) of 10.41 nm. The CoPc ($CoPc_{evap}$) films were deposited on the FTO-coated substrate using vacuum thermal evaporation. AFM analysis of the $CoPc_{evap}$ film shows that the surface has a fine-grained structure with an Ra of 2.56 nm (Figure 2b). The CoPc nanowires ($CoPc_{nws}$) were obtained by the TG-PVD method on the FTO-coated substrate. As seen in Figure 2c, the surface of the film consists of numerous nanosized ribbons covering the entire substrate, with an average width of ≈30 nm.

The preparation of the bilayer films NiO_x/$CoPc_{evap}$ and NiO_x/$CoPc_{nws}$ consisted of two sequential stages. At the first stage, NiO_x films were prepared, and at the next stage, CoPc films or nanowires were synthesized on the surface of the NiO_x film. It is known that during the preparation of the CoPc film by thermal vacuum evaporation, the deposition of molecules onto the substrate surface occurs due to van der Waals interactions. As seen in Figure 2d, the CoPc film forms a thin, uniform structure on the NiO_x surface with an Ra of 3.23 nm. The uniform surface with lower roughness is more favorable for improving the ohmic contact, which can enhance the performance of the solar cell.[28] Moreover, by introducing an additional $CoPc_{evap}$layer, we can improve the quality of NiO_x, reducing its pores and smoothing the surface morphology.

When forming CoPc nanowires on the substrate surface from the vapor phase, the sublimation of phthalocyanine molecules and subsequent condensation of the vapor from the flow of a

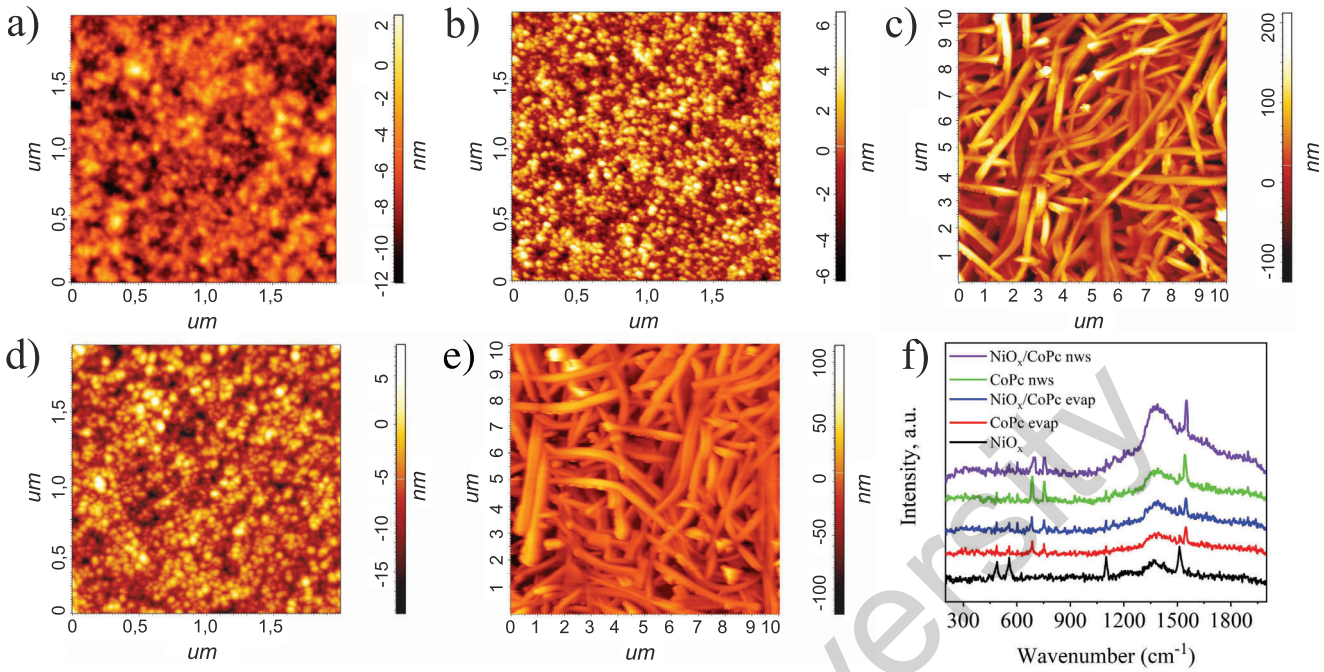

Figure 2. AFM images a–e) and Raman scattering spectra f) of NiO_x films, CoPc films, CoPc nanowires, bilayer $NiO_x/CoPc_{evap}$, and $NiO_x/CoPc_{nws}$ films.

low-pressure inert gas depends on the supersaturation process.[29] By changing the deposition conditions, such as evaporation temperature, substrate temperature, or the inert gas flow rate within the chamber, the degree of vapor supersaturation is modified. Lowering the temperature of the vapor phase along the length of the quartz tube results in the gradient formation of nanowires of varying thickness on the substrate surface. Subsequent growth and self-organization of the molecules on the substrate occur along the molecular axis due to π-π* interactions.[30] In the case of CoPc nanowires synthesized on the NiO_x surface, wider nanowires with a size of approximately ~35 nm are observed (Figure 2e).

AFM images of the surface of perovskite films obtained on the surface of different HTLs are shown in Figure S1 (Supporting Information). The figure shows that when perovskite is deposited on the glass surface, densely arranged crystals with Ra equal to 20.14 nm are observed.When the perovskite layer is deposited on the NiO_x surface, crystal enlargement and an increase in Ra up to 22.99 nm are observed. After applying perovskite on the $NiO_x/CoPc_{evap}$ surface, a decrease in crystal size and Ra to 14.45 nm is observed. For perovskite films on the $NiO_x/CoPc_{nws}$ surface, an inhomogeneous morphology consisting of both large and small crystals with an Ra value of 32.36 nm is observed.

In Figure 2f, the Raman scattering spectra of the samples, recorded with excitation by a laser with λ = 785 nm, are presented. The Raman spectra of NiO_x show four peaks at 540 cm^{-1}, 560 cm^{-1}, 700 cm^{-1}, and 1100 cm^{-1}, which correspond to the five peaks of the vibrational spectrum of NiO_x.[31] These peaks are associated with the first-order (1P) longitudinal optical (LO) phonon mode and the second-order (2P) two-phonon longitudinal optical (2LO) mode. The peaks at 540 cm^{-1} and 560 cm^{-1} correspond to the Ni-O vibrations (one-phonon modes TO and LO), while the peak around 700 cm^{-1} is attributed to the two-phonon 2TO modes. The last most prominent peak at ~1100 cm^{-1} corresponds to the 2LO modes.[32] The observed Raman spectra, with LO and 2TO modes in the nanoscale thin NiO_x films, are quite similar to those in the single crystal. In all Raman spectra of the CoPc films, a main scattering peak at 1545 cm^{-1} is observed, associated with the vibrations of atoms in the C-N-C bridge bonds, characteristic of the metal phthalocyanine structure. Additionally, the spectra show peaks corresponding to the deformation vibrations of the macrocycle C-N (1545 cm^{-1} – B1g mode) and C-C (688 cm^{-1} – A1g and 752 cm^{-1} – B1g modes).[33]

The X-ray diffraction patterns of the studied samples are shown in **Figure 3**. All observed diffraction peaks exhibit pronounced features, indicating the presence of crystalline phases in each sample. The 2θ values for NiO_x correspond to the formation of a face-centered cubic phase (Figure 3a).[34] The crystallite size of the samples was determined from the diffraction peak widths using the Scherrer equation:[35]

$$D = k\lambda/\beta cos\theta \quad (1)$$

where D – crystallite size, K – constant (K = 0.9), λ – the X-ray wavelength, θ – the Bragg difraction angle, β – full width at half maximum (FWHM).

The average crystallite size calculated for the NiO_x samples is 25.6 nm. The diffraction pattern for $CoPc_{nws}$ on NiO_x shows an additional reflection at 7.085°, which is characteristic of CoPc nanowires.[36] The $CoPc_{evap}$ on NiO_x displays two additional reflections at 7.085° and 9.307°. These peaks correspond to the (100) and (102) planes of β-CoPc(Figure 3b).[37] X-ray spectra over a wide range of angles for $NiO_x/CoPc$ films are shown in Figure S2 (Supporting Information).

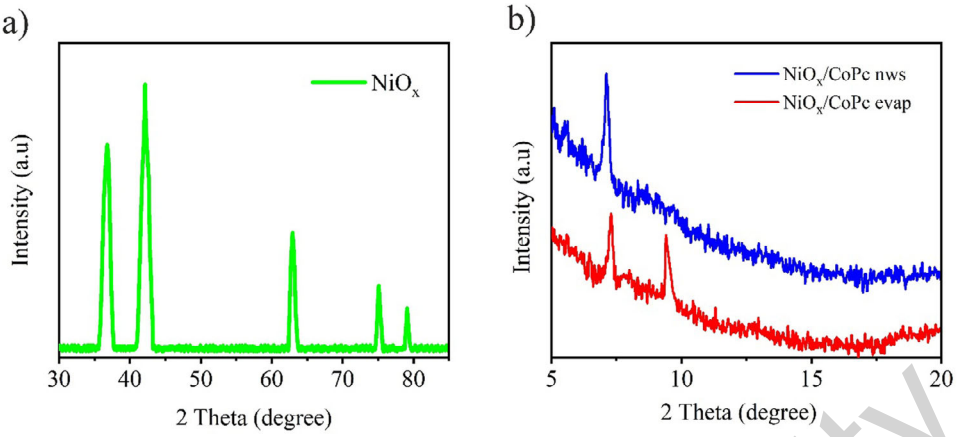

Figure 3. X-ray diffractograms of NiO_x, $NiO_x/CoPc_{evap}$ and $NiO_x/CoPc_{nws}$ films.

3.2. Optical Properties

In **Figure** 4a, the absorption spectra of NiO_x, CoPc films, CoPc nanowires, and composite films $NiO_x/CoPc_{evap}$ and $NiO_x/CoPc_{nws}$ are presented. It is evident from the figure that NiO_x films show good absorption in the short-wavelength region of the visible spectrum. The observed strong absorption in the short-wavelength region corresponds to interband transitions from the valence band to the bottom of the conduction band. This region corresponds to transitions from the final states of the valence band to the broadened states of the conduction band.[38]

The absorption spectra of CoPc films and nanowires show two intense bands in the 300–400 nm range, corresponding to the B-band, and in the 650–700 nm range, corresponding to the Q-band. The B-band is related to mixed π-π* transitions $a_{2u} \rightarrow e_g$ and $b_{2u} \rightarrow e_g$, while the Q-band corresponds to the π-π* transition $a_{1u} \rightarrow e_g$ (Figure 4b).[39] The splitting of the absorption spectra into two peaks in the Q-band is related to Davydov splitting.[40]

In the absorption spectra of the composite films $NiO_x/CoPc_{evap}$ and $NiO_x/CoPc_{nws}$, both NiO_x and CoPc absorptions are observed. However, the B-band overlaps with the absorption corresponding to the interband transition of NiO_x, which results in the

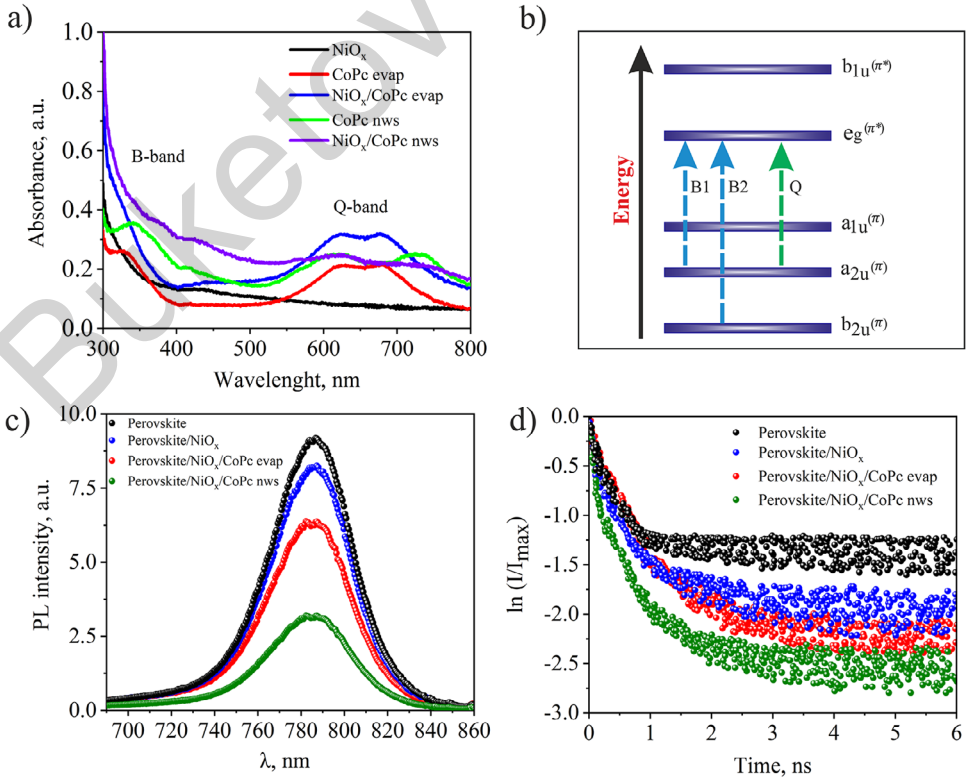

Figure 4. Absorption spectra of films a), electronic transition diagram b), fluorescence c), and fluorescence kinetics (d) of the films.

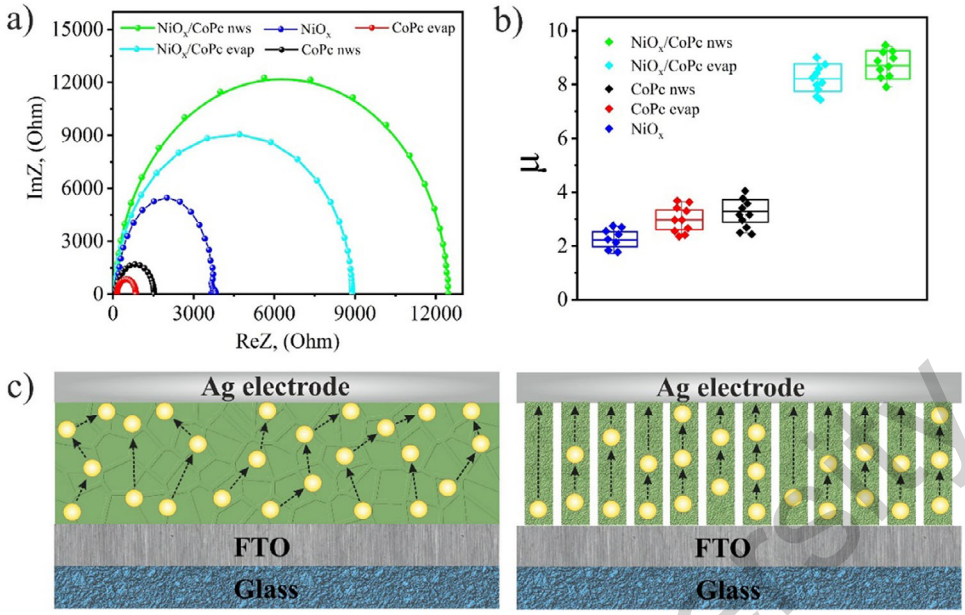

Figure 5. Impedance plot of HTLs films a), electron mobility statistics b) and charge carrier movement diagram c).

absence of this band in the absorption spectrum of the composite films.

Figure 4c shows the fluorescence spectra of perovskite obtained on the surface of different HTLs. It is shown that pure perovskite, directly formed on the glass substrate, exhibits high fluorescence intensity with a peak at a wavelength of $\lambda = 785$ nm. When the fluorescence of perovskite is measured on HTLs, a quenching of fluorescence intensity is observed, indicating efficient charge transfer to the perovskite/HTLsinterface.

For further investigation of carrier recombination processes in perovskite films, we studied fluorescence with time resolution (TRPL), as shown in Figure 4d. Fluorescence kinetics of perovskite films were measured at a wavelength of 780 nm using time-correlated photon counting with excitation by a diode laser (λgen = 640 nm, τ = 150 ps). The fluorescence lifetime was calculated from the linear part of the logarithmic curve for different samples. The experiment showed that the perovskite emission decay follows an exponential decay with τ_{fl} = 1.9 ns. For perovskite/NiO_x films, the fluorescence lifetime decreases to τ_{fl} = 0.9 ns (Figure 4d). For perovskite/NiO_x/$CoPc_{evap}$ films, the fluorescence decay time is τ_{fl} = 0.4 ns. The greatest reduction in lifetime to τ_{fl} = 0.2 ns is observed for the perovskite/NiO_x/$CoPc_{nws}$ films. The quenching of perovskite fluorescence, both in terms of intensity and lifetime, indicates effective charge transfer from the excited perovskite to the conduction band of NiO_x/$CoPc_{nws}$, which is related to high conductivity and appropriate energy alignment.

3.3. Photoelectrical Characterizations

One of the main electrical properties of a semiconductor material is its conductivity, which depends on the mobility of charge carriers. There are several well-established methods for measuring the carrier mobility in films,[41] such as dark current injection with space charge limitation (DI-SCLC), carrier extraction via linearly increasing voltage (CELIV), but the most commonly used method is the measurement of the time of flight of carriers through the sample. However, the requirement for film thickness (greater than 1 μm) limits its application for thin films. Therefore, in this work, we used impedance spectroscopy (IS) to evaluate the electron mobility in the investigated films. **Figure** 5a shows the impedance spectra of the studied cells. **Table** 1 contains the electrical parameters determined from the IS data. The electron mobility was estimated using the following equation:[42]

$$\mu = \frac{e \cdot D_n}{k_B \cdot T} \tag{2}$$

where

$$D_n = \frac{L^2}{\tau_D} \tag{3}$$

Here L is the thickness of the films, $\tau_D = R_t \bullet C$ is the time of electron passage through the investigated film.

As seen in Figure 5a, the use of phthalocyanines leads to an increase in electron mobility in composite films. This trend is associated with the fact that phthalocyanines help passivate surface defects in NiO_x.[43] Figure 5b shows the statistical deviations μ from the average value. Ten cells were fabricated for each type of HTLs, and as shown in the data, the deviations are minimal, amounting to 2.8%.Figure 5c presents the diagrams of charge carrier movement in solid films, produced by vacuum thermal evaporation, and in nanowires, formed by vapor-phase deposition. The solid film obtained by thermal deposition has a domain structure, with a chaotic arrangement of domains within the film. The presence of this domain structure reduces the effective mean free path length of charge carriers (D_n), hindering their movement within the film. This is due to the fact that the defect density

Table 1. Electrical transport parameters of the films.

Samples	R_1,[Ohm]	τ_D,[ps]	D_n, [cm^2,s^{-1}]	C [pF]	μ, [cm^2 V^{-1} s^{-1}]
NiO_x	54.90	275	1.17	5.5	2.3
$CoPc_{evap}$	91.66	458	1.57	5.1	3
$CoPc_{nws}$	79.01	396	1.23	5.2	3.1
$NiO_x/CoPc_{evap}$	37.10	197	4.01	5.3	8.1
$NiO_x/CoPc_{nws}$	20.74	144	4.20	6.9	8.7

at the domain boundaries is significantly higher than in the bulk, and therefore, the increase in the total area of domain boundaries leads to a rise in surface defects, which act as electronic traps.

In the nanowires, the molecules are structured along the molecular axis, forming a lamellar structure. The electron in this case is able to move along the nanowire without encountering obstacles, which is confirmed by the increase in the mean free path length (D_n). Additionally, the effective lifetime (τ_D) decreases.

Figure S3 (Supporting Information) shows the current–voltage characteristics of the solar cells based on $CoPc_{evap}$ and $CoPc_{nws}$ nanostructures. Cells consisting of multiple layers of FTO/CoPc/Ag were prepared for photoelectrophysical measurements. The photoelectric characteristics of the cells are presented in Table S1 (Supporting Information). From the data obtained, it was found that the $CoPc_{nws}$-based photocells exhibited the highest photocurrent compared to the cells based on the $CoPc_{evap}$ film. More charge carriers are generated in $CoPc_{nws}$ due to the broadening of absorption bands in the Q- and B-bands under illumination, compared to $CoPc_{evap}$. As a result, the short-circuit current density (J_{sc}) increases by an average factor of 1.3, and the open-circuit voltage (U_{oc}) increases by 0.2 V. The increase in open-circuit voltage in cells with $CoPc_{nws}$ is associated with a reduction in energy losses.[44] The parameters of the current–voltage characteristics of $CoPc_{nws}$ correlate with changes in the absorption spectra (Figure 4a). The increase in short-circuit current of $CoPc_{nws}$ can also be attributed to several factors, such as reduced recombination of charge carriers in the active layer and enhanced charge carrier transport due to an increased interface area.[45] The current–voltage characteristics of CoPc nanostructures are summarized in Table S1 (Supporting Information).

To confirm the effectiveness of the HTLs films, we fabricated inverted PSCs with the configuration FTO/HTLs/MAPbI3/PC61BM/BCP/Ag (**Figure 6a**). Figure 6b shows the current-voltage characteristics of the inverted PSCs

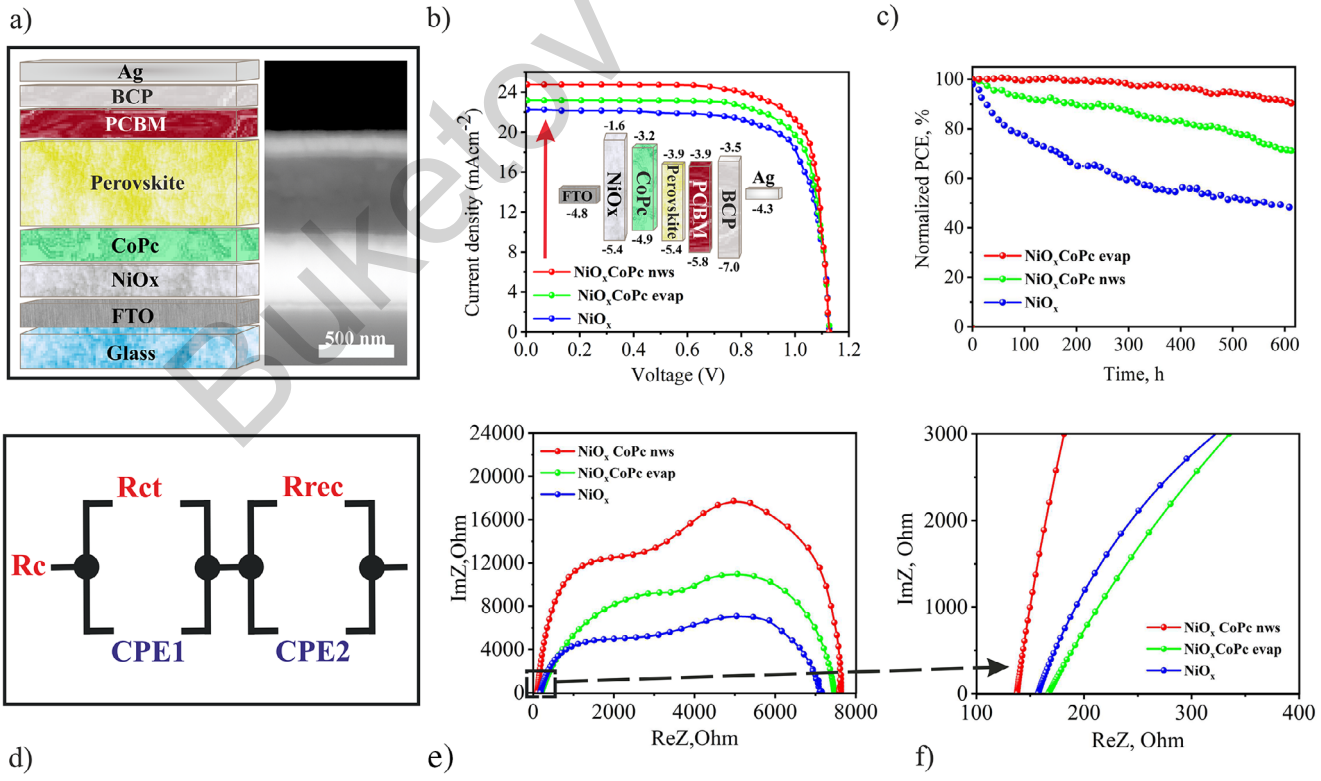

Figure 6. Configuration of PSCs a), I-V characteristics b), stability of PSCs c), equivalent circuit used for the IS setup d), and impedance data for PSCs with different HTLs (e,f).

Table 2. I-V characteristics of PSCs with different HTLs.

Samples	U_{oc} [V]	J_{sc}[mA cm^{-2}]	U_{max}[V]	J_{max}[mA cm^{-2}]	FF %	PCE%
NiO_x	1.12	22.2	0.88	20.5	73	18.1
$NiO_x/CoPc_{nws}$	1.17	24.6	0.95	22.1	73	20.7
$NiO_x/CoPc_{evap}$	1.15	23.1	0.91	21.2	72	19.1

with different HTLs. The energy diagram of the PSCs functional layers is illustrated in the inset of Figure 6b. The diagram was constructed using data reported in references.[46–48] The photovoltaic parameters of the PSCs are shown in **Table 2**. From Table 2, it can be seen that the PSC with the composite HTLs $NiO_x/CoPc_{nws}$ exhibits the highest PCE (20.7%) with a short-circuit current density (Jsc) of 22.2 mA cm^{-2}, an open-circuit voltage (Voc) of 1.17 V, and a fill factor (FF) of 0.73. In comparison, the PSCs with the standard HTLs NiO_x have lower performance with a PCE of 18.1%, Jsc of 22.2 mA cm^{-2}, Voc of 1.12 V, and FF of 0.73. The inverted PSCs with the HTLs $NiO_x/CoPc_{evap}$ show intermediate values with a PCE of 19.1%, Jsc of 23.1 mA cm^{-2}, Voc of 0.91 V, and FF of 0.72.

The stability of the PSCs with different HTLs was tested by measuring the PCE, as shown in Figure 5c. Stability measurements of non-encapsulated PSCs were conducted under continuous illumination using a xenon lamp (AM1.5G) for 600 hours. The stability tests were carried out in a nitrogen-filled glove box at 25 °C and 1% relative humidity. The results show that the PSCs with NiO_x exhibited low stability, and their PCE significantly decreased to 48% of its initial value. The lifespan of the inverted PSCs based on NiO_x remains relatively short, and their long-term operational stability is largely limited by degradation at the NiO_x/perovskite heterojunction. Under constant illumination and subsequent heating, PSCs with the photoactive layer $HAPbI_3$ release free iodine (I3-) and hydroiodic acid (HI), which damage the interface between the perovskite and NiO_x layers, creating a number of defects that form an energy barrier for hole extraction and increase recombination at the interface. These defects lead to a significant reduction in the stability and performance of the inverted PSCs.[49,50] In contrast, the PCE of the PSCs based on $NiO_x/CoPc_{nws}$ showed better stability during the test period, retaining 71% of its initial PCE, while the solar cell based on $NiO_x/CoPc_{evap}$ demonstrated the best stability and managed to retain 90% of its initial PCE. This result indicates that $NiO_x/CoPc_{evap}$ not only improves the performance of the PSCs but also serves as an additional protective layer against the degradation of the perovskite layer.

To better understand the charge transfer and recombination processes in PSCs with different HTLs, impedance spectra of the cells were measured. The model analysis was performed according to the equivalent electrical circuit presented in Figure 6d. Since all functional layers in PSCs, except for HTLs, were fabricated under the same conditions, the observed changes in the I-V characteristics are related to changes in the electrotechnical properties of the HTLs. To understand the influence of composite HTLs on charge transfer and recombination processes in PSCs, the impedance response of the devices was measured and analyzed under small sinusoidal perturbations. The impedance spectra of PSCs with different HTLs are shown in Figure 6e,f. In general, the impedance spectrum consists of two semicircles, which are related to the features of charge transfer in the bulk layer (R_{ct}) and the recombination process at the interface (R_{rec}).[51,52] The high-frequency capacitance (CPE1) represents the capacitance associated with the interface, which can be linked to the dielectric properties of the materials and the depletion region, and is often related to the geometric capacitance of the device.[53] The low-frequency capacitance (CPE2) represents the chemical capacitance, which is associated with the effects of ion accumulation and polarization within the perovskite material. The obtained electrophysical values are presented in **Table 3**.

As expected, the low internal series resistance R_s of the PSCs with $NiO_x/CoPc_{nws}$ composite-based HTLs is R_s = 127.85 Ω, which can be explained by the faster hole extraction at the anode interface. Similarly, lower charge transfer resistance R_{ct} and higher recombination resistance R_{rec} were achieved for this device, suggesting a lower charge recombination rate.

For the device with $NiO_x/CoPc_{evap}$ composite-based HTLs, we observe R_{ct} and R_{rec} compared to the NiO_x-based HTLs. The slight increase in Rs is related to the increase in the overall thickness of the HTLs layer.

Thus, the use of CoPc improves not only the conductivity of NiO_x-based HTLs but also the perovskite/NiO_x interface contact, which enhances hole extraction quality. More importantly, the alignment of energy levels and defect passivation at the NiO_x/CoPc interface contribute to improved charge transfer and suppression of recombination.

4. Conclusion

In conclusion, we developed bilayer HTLs based on NiO_x/CoPc for application in inverted PSCs. As an additional layer between the perovskite and NiO_x, CoPc films and nanowires were used. Surface morphology studies showed that the additional CoPc layer smooths and reduces the number of holes in the NiO_x films. The fluorescence intensity and excited state lifetime of the perovskite films on the bilayer HTLs surface decreased, indicating the presence of additional relaxation channels for excited charge carriers. Carrier mobility measurements in the films showed that the use of CoPc increases the electron mobility in the HTLs. The highest electron mobility was obtained in the $NiO_x/CoPc_{nws}$ films. As a result, the performance of PSCs with $NiO_x/CoPc_{evap}$ and $NiO_x/CoPc_{nws}$-based HTLs showed high efficiencies of 19.1% and 20.7%, which are higher than the PSCs with NiO_x (18.1%). PSCs with $NiO_x/CoPc_{evap}$ and $NiO_x/CoPc_{nws}$-based HTLs demonstrated good stability, retaining 90% of their initial performance over 600 hours. The improvement in PSC performance can be explained by faster hole extraction from the interface, lower charge recombination rates, and the enhancement of HTLs film quality. This study demonstrates that bilayer

Table 3. Values of electrophysical parameters of the films.

Samples	R_s [Ω]	R_{ct} [Ω]	R_{rec}[Ω]	CPE_1	CPE_2
NiO_x	155,31	2669	7133	1,62E-06	3,66E-08
$NiO_x/CoPc_{nws}$	127,85	2597	7649	1,16E-07	9,42E-08
$NiO_x/CoPc_{evap}$	168,03	3637	7470	1,46E-06	6,50E-09

HTLs are effective for improving the efficiency and stability of PSCs, which are key factors for the commercialization of PSCs.

Supporting Information

Supporting Information is available from the Wiley Online Library or from the author.

Acknowledgements

This research is funded by the Science Committee of the Ministry of Science and Higher Education of the Republic of Kazakhstan (Grant No. AP19679938).

Conflict of Interest

The authors declare no conflict of interest.

Author Contributions

M.K.B. performed methodology, investigation, formal analysis, data curation, supervision, resources. A.K.A.wrote – review and edited the original draft, formal analysis, conceptualization. S.K.T. wrote – review and edited the original draft, methodology, investigation, formal analysis, data curation, supervision, resources. D.R.A.performed methodology, data curation, supervision, resources. A.K.Z. wrote – review and edited the original draft, project administration, formal analysis, conceptualization.

Data Availability Statement

The data that support the findings of this study are available from the corresponding author upon reasonable request.

Keywords

cobalt phthalocyanine, electrical transport characteristics, hole transport layers, nickel oxide, optical properties, perovskite solar cells

Received: February 12, 2025
Revised: May 31, 2025
Published online: June 23, 2025

[1] M. González-Hernández, S. Reyes, E. Erazo, P. Ortiz, M. Cortés, *Sol. Energy* **2024**, *276*, 112657.
[2] Y.-H. Seo, I. Cho, S.-I. Na, *J. Alloys Compd.* **2019**, *797*, 1018.
[3] J. Su, G. Zheng, B. Chen, P. Dong, B. Ma, D. Yao, N. Tian, Y. Peng, J. Wang, F. Lon, *ACS App. Mater. Interf.* **2024**, *16*, 22761.
[4] F. Ma, Y. Zhao, J. Li, X. Zhang, H. Gu, J. You, *J.Energy Chem* **2021**, *52*, 393.
[5] L. Xu, X. Chen, J. Jin, W. Liu, B. Dong, X. Bai, H. Song, P. Reiss, *Nano Energy* **2019**, *63*, 103860.
[6] M. Yi, W. Jang, D. H. Wang, *ACS Sustain. Chem. Eng.* **2019**, *7*, 8245.
[7] L. Hu, J. Fu, K.e Yang, Z. Xiong, M. Wang, B.o Yang, H. Wang, X. Tang, Z. Zang, M. Li, J. Li, K. Sun, *Sol. RRL* **2019**, *3*, 1900104.
[8] J. H. Park, J. Seo, S. Park, S. S. Shin, Y. C. Kim, N. J. Jeon, H.-W. Shin, T. K. Ahn, J. H. Noh, S. C. Yoon, C. S. Hwang, S. I.l Seok, *Adv.Mater.* **2015**, *27*, 4013.
[9] W. Chen, Y. Zhou, G. Chen, Y. Wu, B. Tu, F.-Z. Liu, L.i Huang, A. M. C. Ng, A. B. Djurisic, Z. He, *Adv. Energy Mater.* **2019**, *9*, 1803872.
[10] H. Sheng, Q. Zhao, X. Sun, B. Zhang, Q. Huang, K. Wang, L. Wang, Sh. Pang, *Sol. RRL* **2023**, *8*, 2300779.
[11] P. Gostishchev, L. Luchnikov, O. Bronnikov, V. Kurichenko, D. Muratov, A. Aleksandrov, A. Aleksandrov, E. Statnik, A. Korsunsky, A. Tameev, M. Tiukhova, T. Le, I. Badurin, M. Ryabtseva, D. Saranin, A. Carlo, *ACS App. Ener. Mater.* **2024**, *7*, 821.
[12] S. Li, X. Wang, N. Huang, S. He, L. Qiu, Y. Qi, *Energy Chem* **2024**, *7*, 100135.
[13] S. Reyes, M. González-Hernández, M. Cortés, P. Ortiz, *Surf. Interfaces* **2025**, *56*, 105564.
[14] W. Chang, H. Tian, G. Fang, D. Guo, Z. Wang, K. Zhao, *Sol. Energy* **2019**, *186*, 323.
[15] Y. Wang, S. Akel, B. Klingebiel, T. Kirchartz, *Adv. Energy Mater.* **2023**, *14*, 2302614.
[16] S. Mali, J. Patil, H. Kim, R. Luque, C. Hong, *Mater. Today* **2019**, *26*, 8.
[17] R. Li, P. Wang, B. Chen, X. Cui, Y. Ding, Y. Li, D. Zhang, Y. Zhao, X. Zhang, *ACS Energy Lett.* **2019**, *5*, 79.
[18] H. Sun, K. Deng, Y. Zhu, M. Liao, J. Xiong, Y. Li, L. Li, *Adv. Mater.* **2018**, *30*, 1801935.
[19] X. Yin, J. Zhai, L. Song, P. Du, N. Li, Y. Yang, J. Xiong, F. Ko, *ACS Appl. Mater. Interf.* **2019**, *11*, 44308.
[20] G. Yang, Y.u-L. Wang, J.-J.u Xu, H.-W. Lei, C. Chen, H.-Q. Shan, X.-Y. Liu, Z.-X. Xu, G.-J. Fang, *Nano Energy* **2017**, *31*, 322.
[21] T. Duong, J. Peng, D. Walter, J. Xiang, H. Shen, D. Chugh, M. Lockrey, D. Zhong, J. Li, K. Weber, T. P. White, K. R. Catchpole, *ACS Energy Lett.* **2018**, *3*, 2441.
[22] Z. Yu, L. Wang, X. Mu, C. C. Chen, Y. Wu, J. Cao, Y. Tang, *Angew. Chem., Int. Ed.* **2021**, *60*, 6294.
[23] J. Han, Y. Tu, Z. Liu, X. Liu, H. Ye, Z. Tang, T. Shi, G. Liao, *Electrochim. Acta* **2018**, *273*, 273.
[24] M. Haider, C. Zhen, T. Wu, J. Wu, C. Jia, G. Liu, H.-M. Cheng, *Chem. Commun.* **2019**, *55*, 5343.
[25] X. Zhao, W. Zhang, X. Feng, X. Guo, C. Lu, X. Li, J. Fang, *Chem. Eng. J.* **2022**, *435*, 135140.
[26] J. D. Wright, *Prog. Surf. Sci.* **1989**, *31*, 1.
[27] J. Bisquert, I. Mora-Sero, F. Fabregat-Santiago, *Chem. Electro. Chem.* **2013**, *1*, 289.
[28] A. Qureshi, E. Schütz, S. Javed, L. Schmidt-Mende, A. Fakharuddin, *Energy Adv.* **2023**, *2*, 1905.
[29] A. Pinjari, D. Saraf, D. Sengupta, *Phys. Chem. Chem. Phys.* **2023**, *25*, 30259.
[30] R. Saini, A. Mahajan, R. K. Bedi, D. K. Aswal, A. K. Debnath, *Sens. and Actu. B: Chem.* **2014**, *203*, 17.

[31] B. Bhushan, *Microsyst. Technol.* **2017**, *23*, 1595.
[32] A. Bouhank, Y. Bellal, H. Serrar, *J. Chem. Chem. Eng.* **2018**, *12*, 116.
[33] M. Szybowicz, W. Bała, K. Fabisiak, K. Paprocki, M. Drozdowski, *Cryst. Res. Technol.* **2010**, *45*, 1265.
[34] S. A. Mahmoud, S. Alshomer, M. A. Tarawnh, *J. Mod. Phys.* **2011**, 1178.
[35] K. Mongkolsuttirat, J. Buajarern, *J. Phys.* **2021**, *1719*, 012057.
[36] S. Tazhibayev, A. Zeinidenov, X. Rozhkova, A. Zhakanova, A. Aimukhanov, T. Mukametkali, V. Paygin, D. Valiev, *Mater. Chem. Phys.* **2023**, *301*, 127696.
[37] Mounesh, P. Malthesh, N. Y. Praveenkumar, B. S. Jilani, C. D. Mruthyunjayachari, K. R. Venugopala Reddy, *Heliyon* **2019**, *5*, 01946.
[38] T. Ivanova, A. Harizanova, M. Shipochka, P. Vitanov, *Opt. Electr. Prop. Mater.* **2022**, *15*, 1742.
[39] M. S. Liao, S. Scheiner, *J. Chem. Phys.* **2001**, *114*, 9780.
[40] M. M. El-Nahass, F. S. Bahabri, A. A. AL Ghamdi, S. R. Al-Harbi, *Egypt. J. Solids* **2001**, *25*, 307.
[41] Q. Ji, H. Yang, J. Li, R. Wang, C. Zhang, *Phys. Chem. C* **2024**, *128*, 10520.
[42] A. Kokil, K. Yang, J. Kumar, *J. Polymer Sci. Part B* **2012**, *50*, 1130.
[43] X. Yin, J. Zhai, L. Song, P. Du, N.i Li, Y. Yang, J. Xiong, F. Ko, *ACS Appl. Mater.Interf.* **2019**, *11*, 44308.
[44] V. Singh, R. Singh, B. Parthasarathy, A. Aguilera, J. Anthony, M. Payne, *Appl. Phys. Lett.* **2005**, *86*, 082106.
[45] A. K. Aimukhanov, A. K. Zeinidenov, A. Zavgorodniy, *Opt. Mater.* **2021**, *116*, 111099.
[46] T. Liu, K. Chen, Q. Hu, R. Zhu, Q. Gong, *Adv. Energy Mater.* **2016**, *6*, 1600457.
[47] N. Tiwari, H. Dewi, E. Erdenebileg, R. Chauhan, N. Mathews, S. Mhaisalkar, A. Bruno, *RRL Solar* **2022**, *6*, 2100700.
[48] Z. Yu, L. Wang, X. Mu, C. Chen, Y. Wu, J. Cao, Y. Tang, *Angew. Chem., Int. Ed.* **2021**, *60*, 6294.
[49] R. S. Kate, S. C. Bulakhe, R. J. Deokate, *J. Electron. Mater.* **2019**, *48*, 3220.
[50] A. A. Yadav, U. J. Chavan, *J. Electroanal. Chem.* **2016**, *782*, 36.
[51] W. Clarke, G. Richardson, P. Cameron, *Adv. Energy Mater.* **2024**, *14*, 2400955.
[52] A. Pockett, G. Eperon, T. Peltola, H. Snaith, A. Walker, L. Peter, P. Cameron, *Chem. C Article Phys. Chem.* **2015**, *119*, 3456.
[53] A. Ghoudi, K.h. Ben Brahim, H. Ghalla, J. Lhoste, S. Auguste, K. Khiroun, A. Aydi, A. Oueslati, *RSC Adv.* **2023**, *13*, 12844.

